Electronic Supplementary Information

Dual Emission N-doped Carbon Dots@Benzotrithiophene Tricarbalaldehyde-Terephthalic Dihydrazide Covalent Organic Framework

Yonghai Song, Lulu Guo, Yue Du, Li Yang and Li Wang*

Key Laboratory of Functional Small Organic Molecule, Ministry of Education, Key Laboratory of Chemical Biology, Jiangxi Province, College of Chemistry and Chemical Engineering, Jiangxi Normal University, Nanchang, 330022, China

*Corresponding author: Tel/Fax: +86 791 88120861. E-mail: lwang@jxnu.edu.cn (L. Wang).

Materials and methods

Benzotrithiophene tricarbaldehyde (BTT) and terephthalic dihydrazide (Th) were obtained from Jilin Chinese Academy of Sciences-Yanshen Technology Co., Ltd. (Changchun, China). Urea was purchased from Sigma-Aldrich. $Hg(NO_3)_2$, $MgCl_2$, $Zn(NO_3)_2$, $Pb(NO_3)_2$ and $CuSO_4$ were purchased from Sinopharm Chemical Reagent Co., Ltd (Shanghai, China). Anhydrous citric acid and N-2-hydroxyethylpiperazine-N'-2-ethanesulfonic acid (HEPES) were obtained from Aladdin Industrial Corporation (Shanghai, China). Other reagents were obtained from Guangdong Xilong Chemical Reagent Factory (Guangzhou, China). All solutions were prepared with ultra-pure water, purified by a Millipore-Q system (18.2 MΩ cm^{-1}). HEPES buffer (25 mM, pH=6.0) was prepared with ultra-pure water and adjusted pH value with 1 M NaOH. All reagents were of analytical grade.

Instrumentation

The measurements of excitation and emission spectra were performed on a Hitachi F-7000 fluorescence spectrophotometer. UV-vis adsorption spectra were measured on a Hitachi U3900-H ultraviolet spectrophotometer. Transmission electron microscopy (TEM) images were obtained via JEOL JEM-2100 microscopes at an acceleration voltage of 200 KV. Scanning electron microscopy (SEM) images were obtained by HITACHI S-3400N SEM at 15 kV. X-ray diffraction (XRD) data were collected on a D/Max 2500 V/PC X-ray powder diffractometer using Cu Kα radiation (λ=1.54056 Å, 40 kV, 200 mA). An ESCALAB 250Xi spectrometer was applied to X-ray photoelectron spectroscopy (XPS) analysis. N_2 adsorption/desorption isotherm measurements were operated using a BELSORP-mini II instrument under the liquid nitrogen temperature (77 K). Perkin-Elmer Spectrometer 200 spectrometer (Perkin-Elmer Company) was utilized to get Fourier transform-infrared spectroscopy (FTIR). Thermogravimetric analysis (TGA) was carried out on

SDT 2960 at a ramping rate 10 ºC min^{-1} in air.

Synthesis of NCDs

Anhydrous citric acid (0.5 g) and urea (0.5 g) were dissolved in 10 mL ultra-pure water and then the solution was transferred into Teflon-lined autoclave chamber. The reactor was placed in an oven and heated at 160 °C for 4 h. After the chamber was cooled down to room temperature, 30 mL acetone was added into the reaction solution. NCDs were then obtained by centrifugation, and the black-green precipitates were collected and dried under vacuum.[1]

Synthesis of COF_{BTT-Th} and NCDs@COF_{BTT-Th}

COF_{BTT-Th} was prepared according to previous method.[2] In short, BTT (66.0 mg, 0.2 mmol) and Th (58.2 mg, 0.3 mmol) was dissolved in mixture of mesitylene/1,4-dioxane (3 mL/3 mL) and then acetic acid (6 M, 0.4 mL) was added as catalyst. After ultrasonication for 10 min, the solution was transferred to the reaction kettle and reacted at 120 °C for 3 days. The precipitation was collected by centrifugation at 10000 rpm and washed with N,N-dimethylformamide and tetrahydrofuran for 3 times alternately to remove those unreacted reagents. Finally, the yellow sediment was dried in vacuum freeze dryer for 12 h. The NCDs@COF_{BTT-Th} was prepared in similar procedures as COF_{BTT-Th}, except that NCDs (30 mg) was added to the precursor of COF_{BTT-Th}.

Fluorescence measurements

The fluorescence properties of NCDs@COF_{BTT-Th} were explored at room temperature. 1.0 mg NCDs@COF_{BTT-Th} was re-dispersed in 1000 mL HEPES buffer (25 mM, pH=7.0). After mixing, the concentration of NCDs@COF_{BTT-Th} was 1 mg·L^{-1}. In fluorescent titration test, a standard solution of Fe^{3+} was added to the probe solution. The emission spectra were recorded at 300 nm excitation wavelength. Emission peak at 547 nm were monitored for analysis.

The NCDs@COF_{BTT-Th} as fluorescence probe to detect Fe^{3+}

Fe^{3+} is one of the essential transition metal ions in the biological system and plays a vital role in the organism.[3] Both deficiency and overdose of Fe^{3+} would cause various functional disorders in the body.[4] For example, Fe^{3+} deficiency can affect the catalysis of hemoglobin producing enzymes and the catalysis of enzymes, which would lead to anemia, decreased immunity and mental disorders.[5] However, excessive Fe^{3+} uptake can lead to the generation of reactive oxygen species, which would cause damage to nucleic acids, lipids, etc., resulting in hepatitis, organ failure, and neurodegenerative diseases.[6] Therefore, finding an efficient, simple and rapid method to detect Fe^{3+} is of particular significance for the early identification and prevention of these diseases. Here, the dual emission NCDs@COF_{BTT-Th} was firstly used a fluorescence probe to detect Fe^{3+}.

In order to obtain the optimal detection result by using NCDs@COF_{BTT-Th} as fluorescence probe, the amount of NCDs and reaction conditions of NCDs@COF_{BTT-Th} were optimized. The process of optimizing the addition of NCDs and the detection conditions were shown in Fig. S6 and Fig. S7 (Supporting Information). As shown in Fig. S6 (Supporting Information), 30 mg was selected as the optimal addition of NCDs in the reaction system of NCDs@COF_{BTT-Th} because more NCDs could not increase the fluorescence intensity at 547 nm. As shown in Fig. S7a,b (Supporting Information), 0.09 mg mL^{-1} NCDs@COF_{BTT-Th} was selected as the appropriate concentration and 300 nm was chosen as the excitation wavelength because the fluorescence intensity at 547 nm was maximum. To get better experimental results, pH of the solution and the reaction time were also explored. As shown in Fig. S7c (Supporting Information), when the pH was increased from 3 to 7, the fluorescence intensity of NCDs@COF_{BTT-Th} also increased gradually, and then the fluorescence decreased with the further increased pH. When the pH value was 7, the fluorescence intensity reached the maximum, so the pH 7 was the best condition for fluorescence detection. From the

curve graph of reaction time (Fig. S7d, Supporting Information), the fluorescence intensity was observed to be decreased significantly within 1 min after the addition of detection Fe^{3+}, and remained unchanged after 1 min, indicating that the reaction time was very quick and could meet the requirement of rapid detection of Fe^{3+} .

Fe^{3+} was detected by NCDs@COF_{BTT-Th} under the optimal experimental conditions. The detection results are shown in Fig S8a. The NCDs@COF_{BTT-Th} fluorescence probe had the most obvious fluorescence response to Fe^{3+} at 547 nm, so the fluorescence peak at 547 nm was recorded and used to observe the fluorescence intensity change after the addition of Fe^{3+}. With the increase of Fe^{3+} concentration, the fluorescence peak intensity both of NCDs and at 547 nm decreased regularly. As can be seen from Fig. S8b, there was a good linear relationship between the fluorescence responses and Fe^{3+} concentration of 10.21 nM -24 μM. The detection limit was 3.40 nM when the SNR was 3.

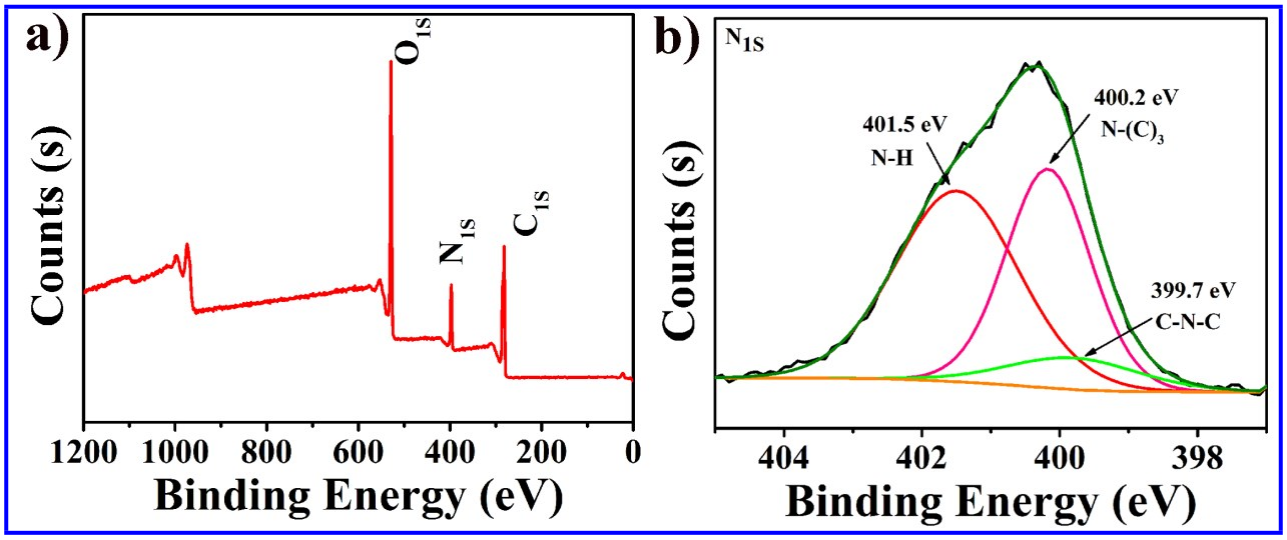

Fig. S1. (a) XPS spectrum of NCDs, and (b) high-resolution XPS spectra of N1s of NCDs.

XPS spectrum of NCDs (Fig. S1a) shows the existence of C, N, O elements in NCDs. The high-resolution XPS shows three peaks at 399.7 eV, 400.2 eV and 401.5 eV which are attributed to The C-N-C, N-$(C)_3$- and N-H groups, respectively.

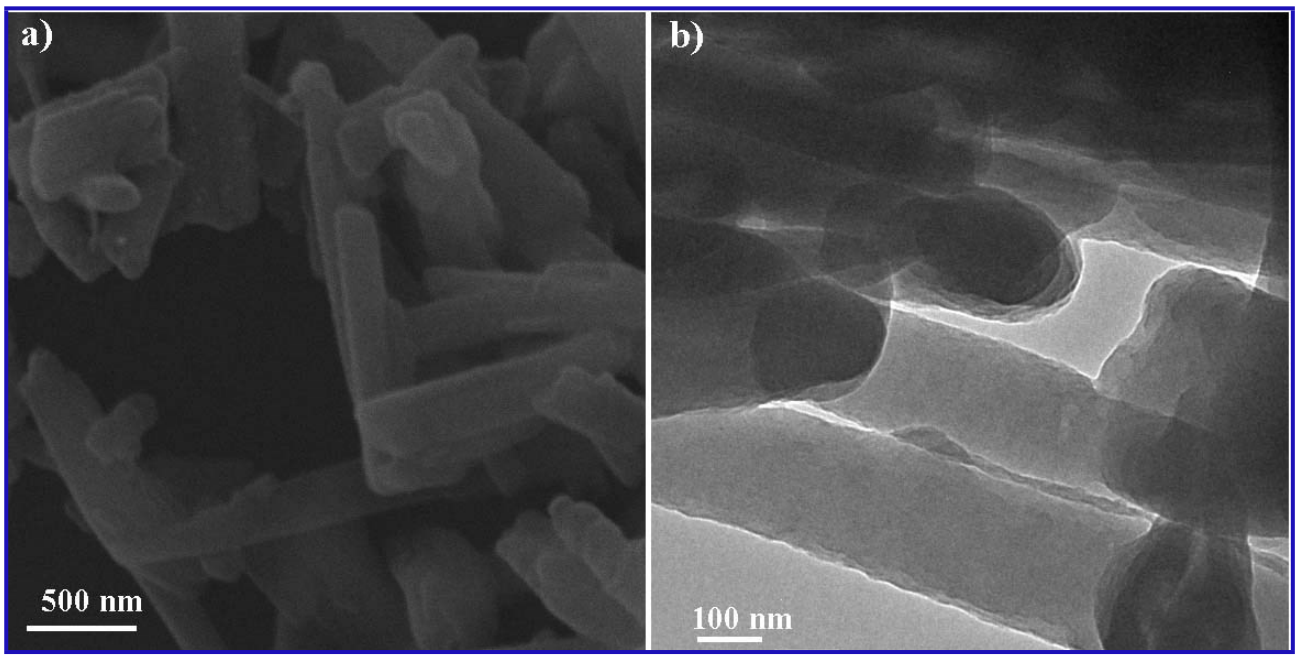

Fig. S2. SEM image and TEM image of $COF_{BTT\text{-}Th}$.

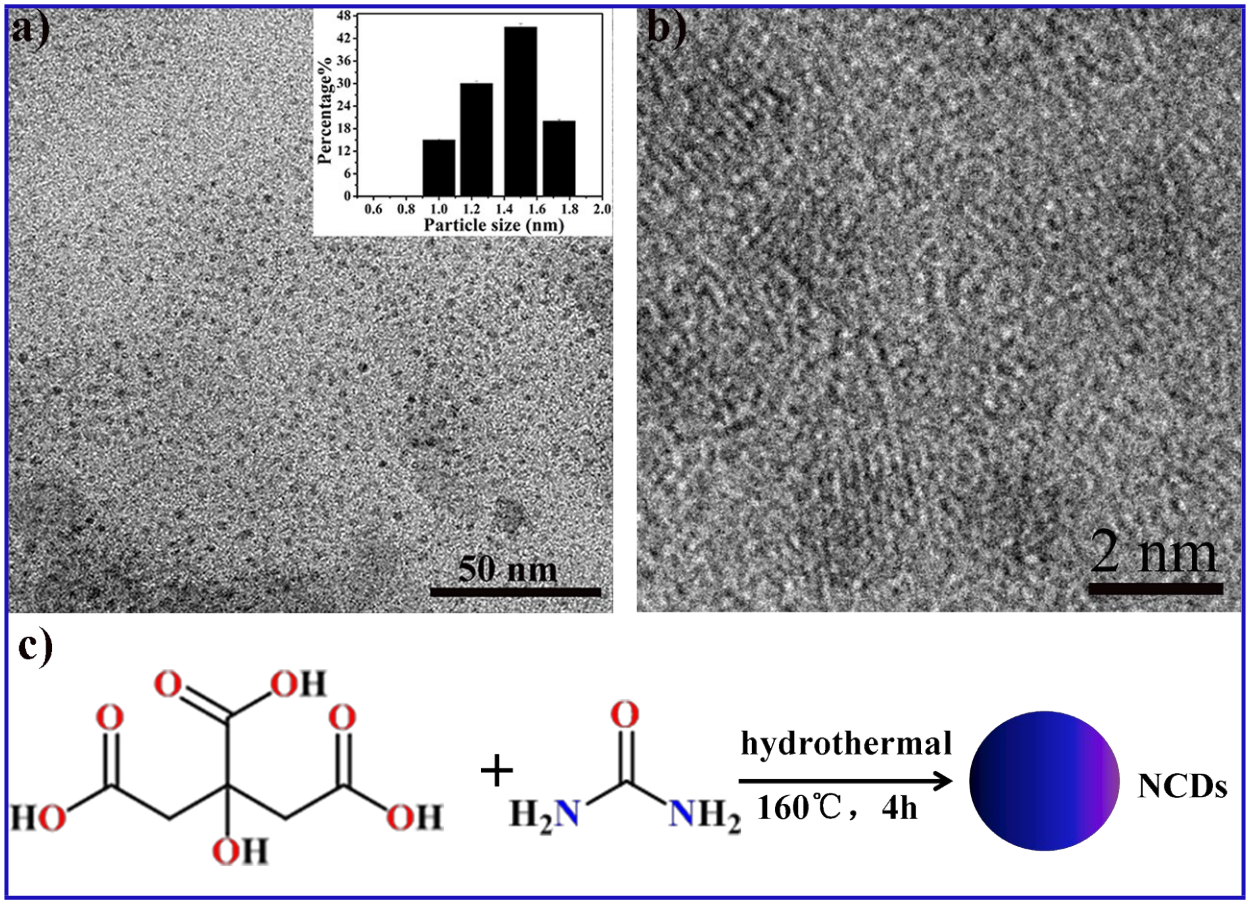

Fig. S3. a) TEM image of NCDs (inset: size distribution). b) High magnification TEM image of NCDs. c) The synthetic route of NCDs.

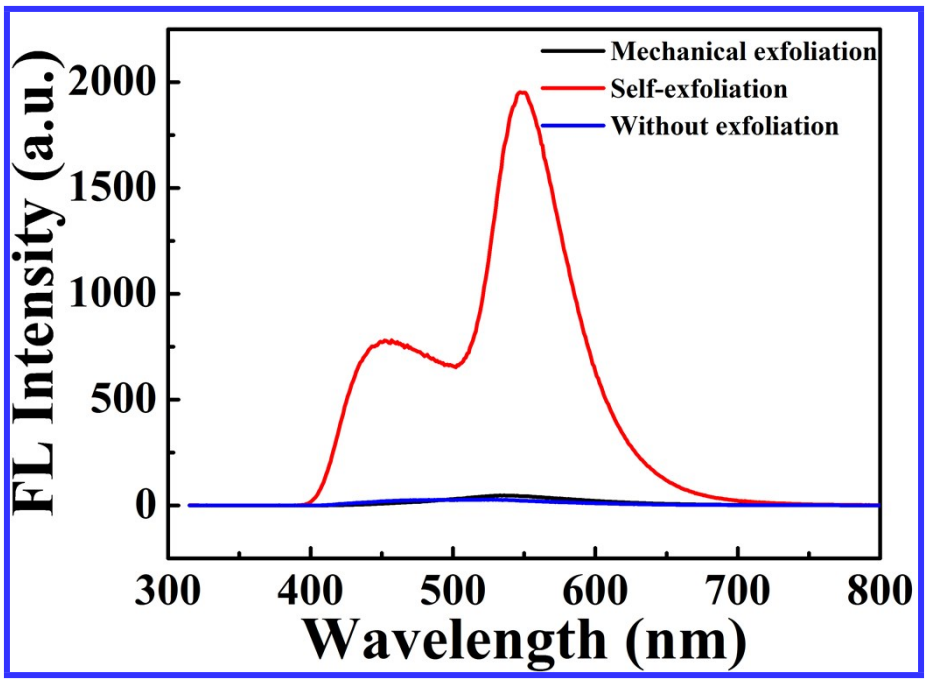

Fig. S4. Fluorescence spectra of $COF_{BTT\text{-}Th}$ under different exfoliation conditions.

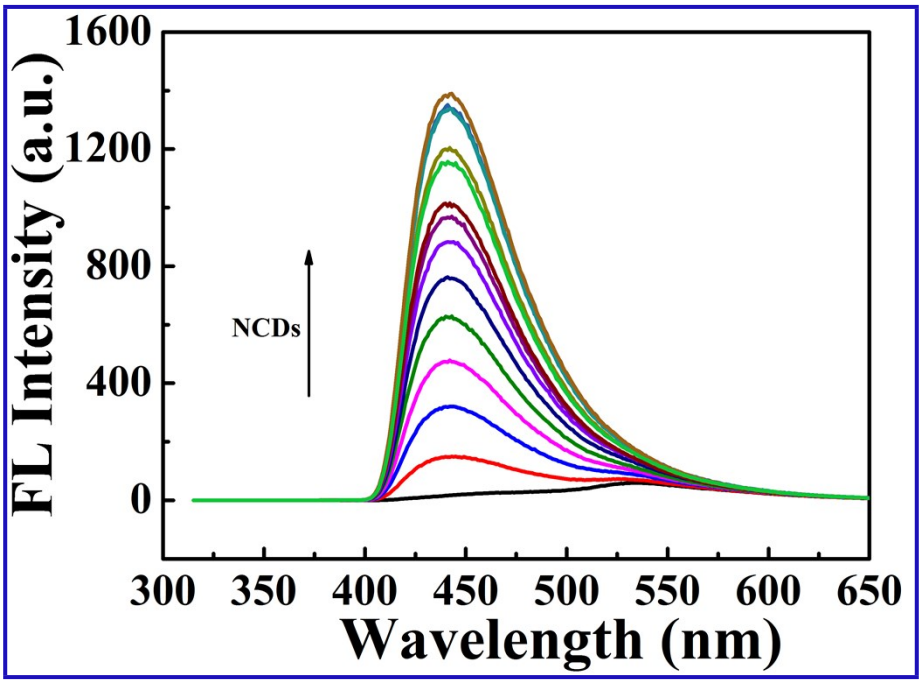

Fig. S5. Titration experiment was conducted to determine the change of COF_{BTT-Th} fluorescence intensity after adding different amounts of NCDs.

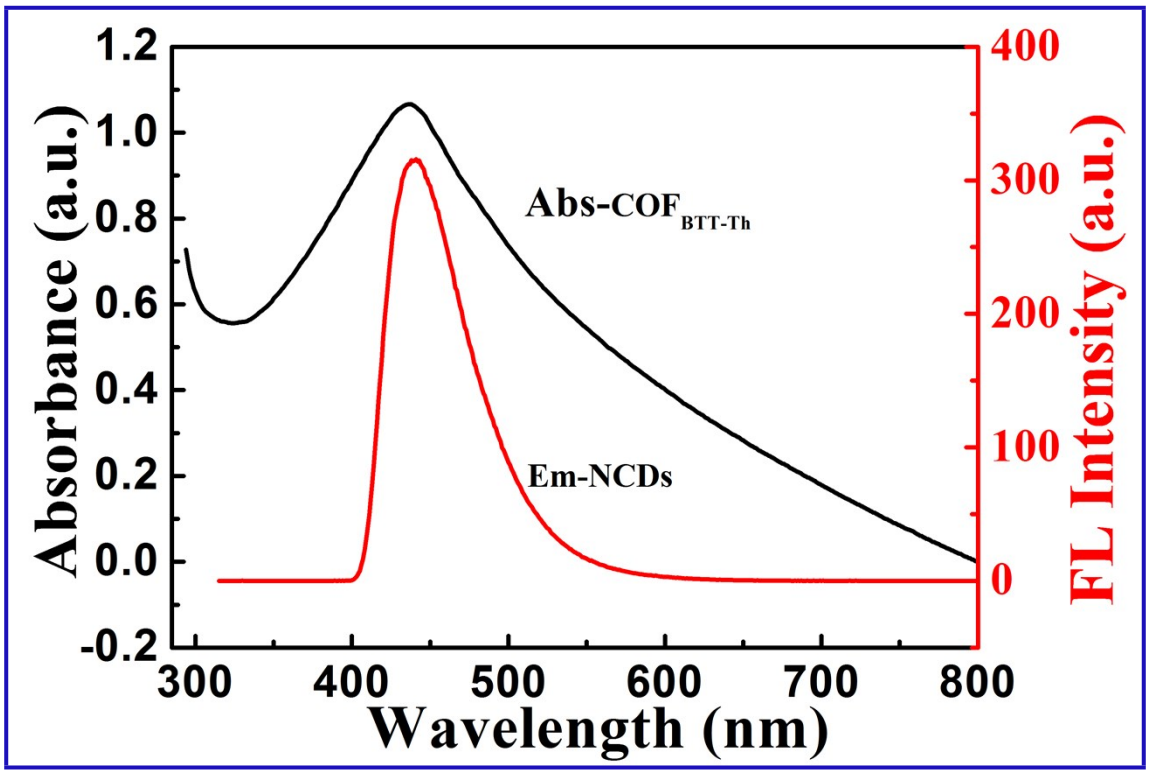

Fig. S6. UV-vis absorption spectra of COF_{BTT-Th} and fluorescence emission of NCDs (λ_{ex}=300 nm).

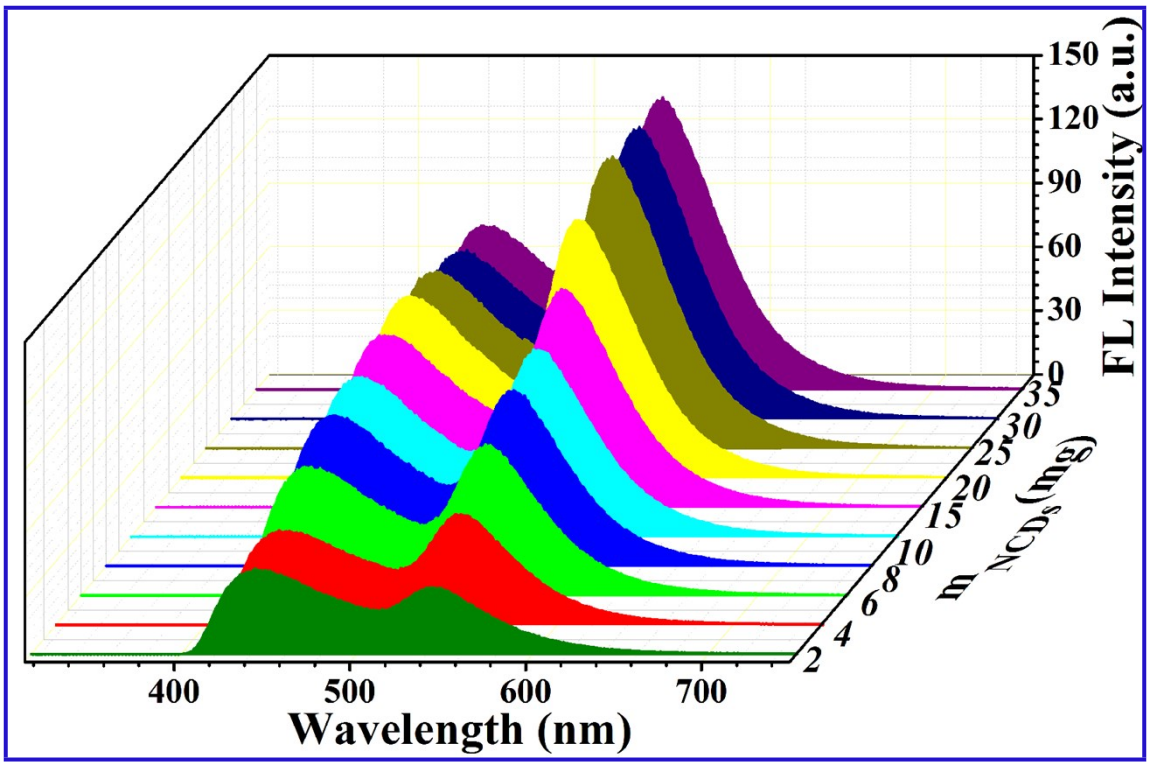

Fig. S7. Fluorescence spectra of NCDs@COF_{BTT-Th} with different NCDs content.

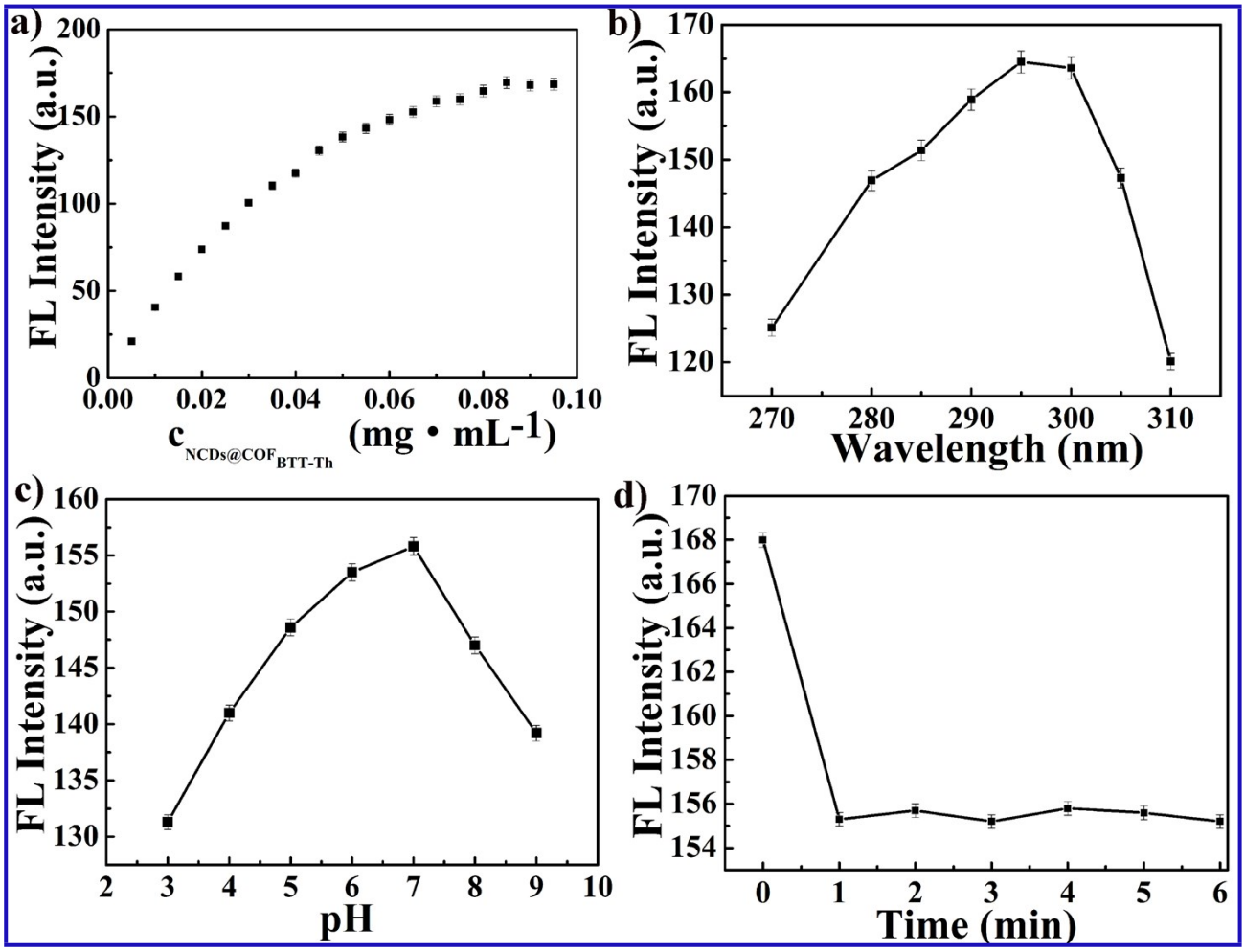

Fig. S8. a) Linear graph of the fluorescence intensity to different concentration of NCDs@COF_{BTT-Th}. b) Fluorescence intensity of NCDs@COF_{BTT-Th} at different excitation wavelengths. c) Effect of pH value of solution on fluorescence intensity of NCDs@COF_{BTT-Th} (300 nm excitation). d) Effect of the reaction time between NCDs@COF_{BTT-Th} and Fe^{3+} on fluorescence intensity of NCDs@COF_{BTT-Th}.

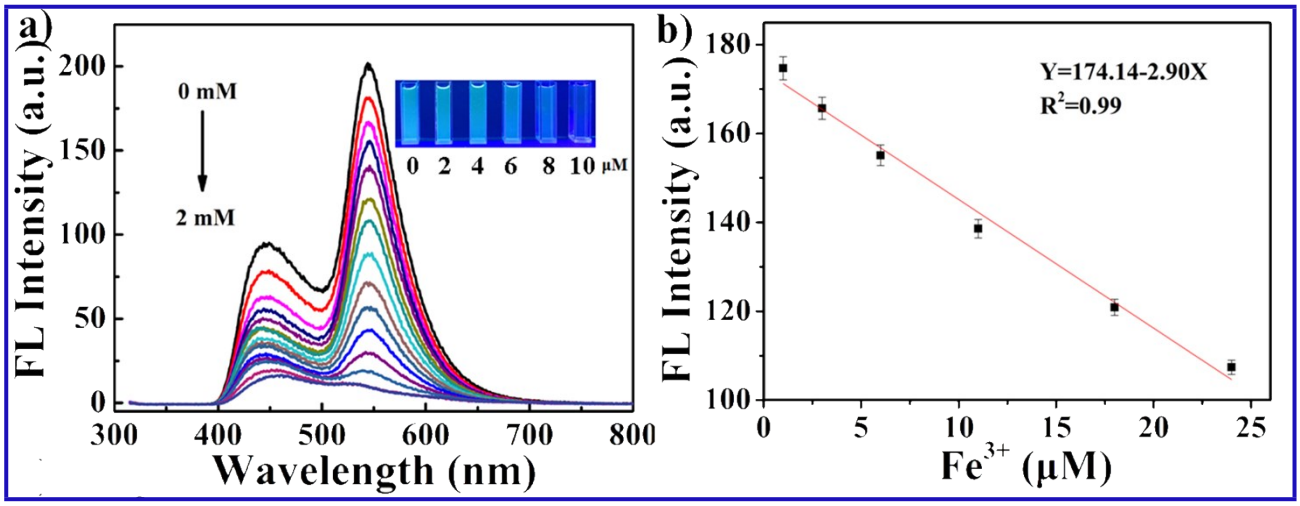

Fig. S9. a) Fluorescence emission spectra of NCDs@COF_{BTT-Th} in the presence of Fe^{3+} with different concentration. b) Linear relationship of the fluorescence intensity of NCDs@COF_{BTT-Th} with Fe^{3+}concentration.

Fe^{3+} was detected by NCDs@COF_{BTT-Th} under the optimal experimental conditions. The detection results are shown in Fig S8a (Supporting Information). The NCDs@COF_{BTT-Th} fluorescence probe had the most obvious fluorescence response to Fe^{3+} at 547 nm, so the fluorescence peak at 547 nm was recorded and used to observe the fluorescence intensity change after the addition of Fe^{3+}. With the increase of Fe^{3+} concentration, the fluorescence peak intensity both of NCDs and at 547 nm decreased regularly. As can be seen from Fig. S8b (Supporting Informaiton), there was a good linear relationship between the fluorescence responses and Fe^{3+} concentration of 10.21 nM -24 μM. The detection limit was 3.40 nM when the SNR was 3.

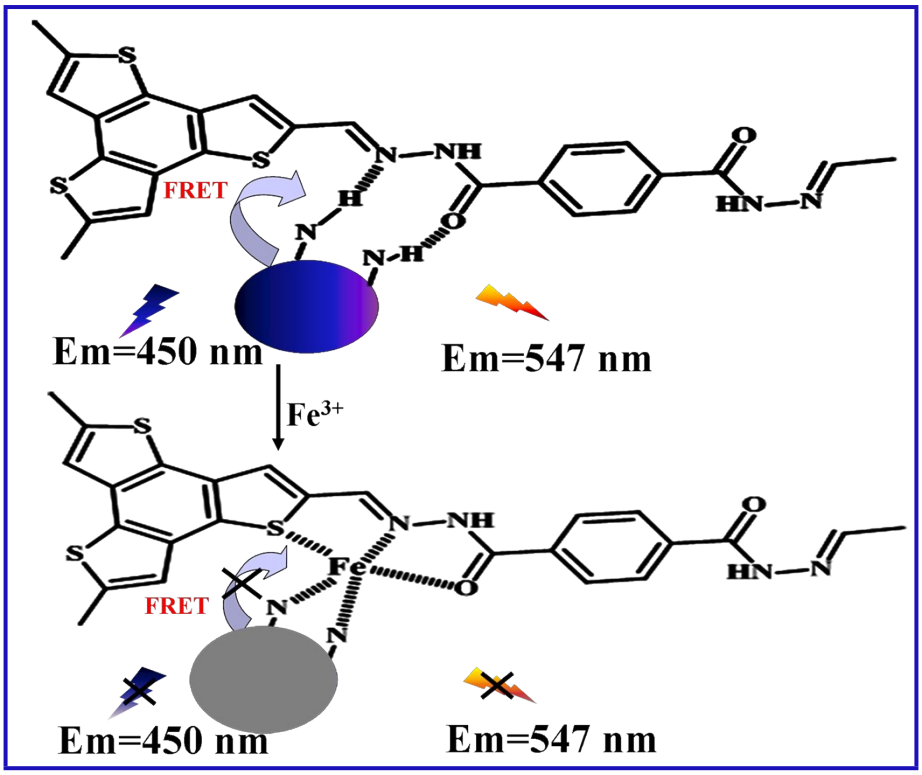

Fig. S10. The reaction mechanism diagram of Fe^{3+} and NCDs@COF_{BTT-Th}.

As shown in Scheme 1, the COF_{BTT-Th} contains a large amount of O, N and S heteroatoms. Therefore, the Fe^{3+} with the void d orbit could coordinate with O,N and S heteroatoms of COF_{BTT-Th}, which blocked the fluorescence resonance energy transfer between NCDs and COF_{BTT-Th} (Fig. S9, Supporting Informaiton).

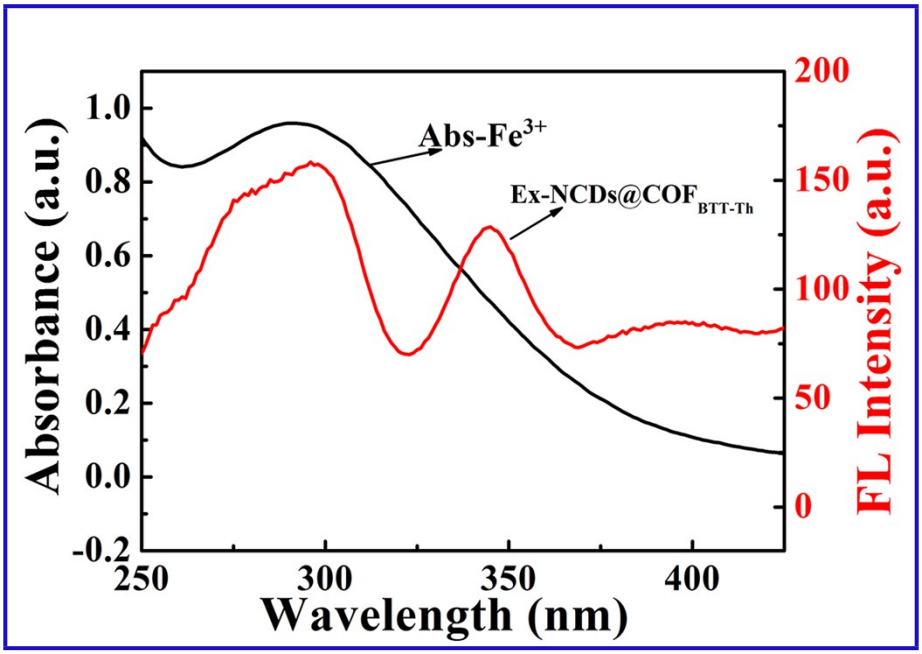

Fig. S11. Ultraviolet absorption of Fe^{3+} and fluorescence excitation of NCDs@COF_{BTT-Th}.

As shown in Fig. S10 (Supporting Information), the fluorescence quenching caused by Fe^{3+} might also result from the internal filtration effect because the excitation spectrum of NCDs@COF_{BTT-Th} overlapped the absorption spectrum of Fe^{3+}.

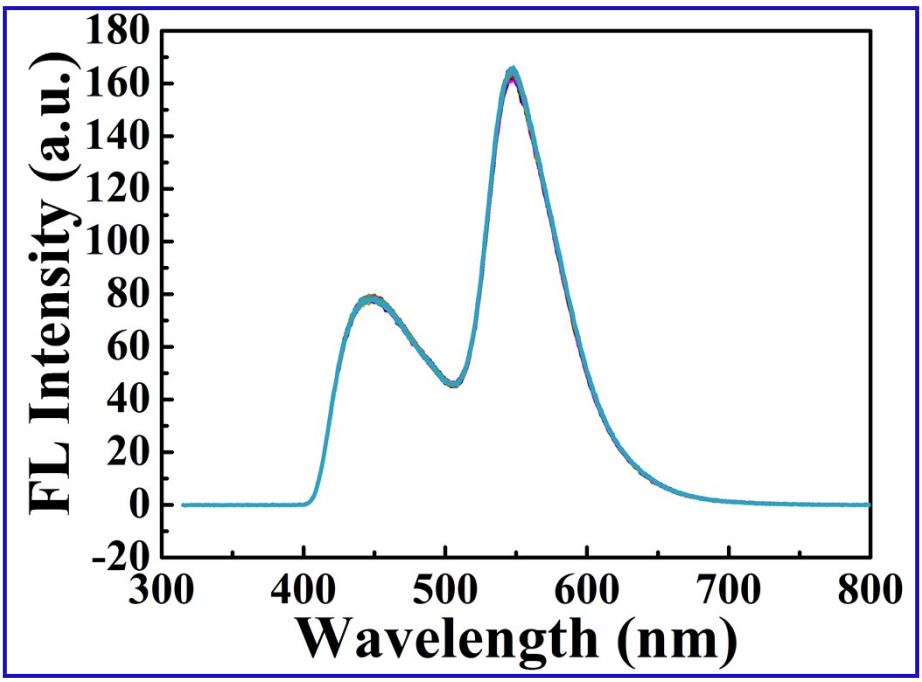

Fig. S12. The fluorescence intensity of NCDs@COF_{BTT-Th} material was measured continuously for 20 min.

Stability and selectivity were important factors to be considered in the practical application of NCDs@COF_{BTT-Th} fluorescence probe. Fig. S11 (Supporting Information) showed the fluorescence intensity of NCDs@COF_{BTT-Th} measured within 20 min continuously. The fluorescence intensity of NCDs@COF_{BTT-Th} had little change within 20 min. The good stability might be ascribed to the 2D porous nanosheet structure of NCDs@COF_{BTT-Th}. The porous 2D structure enabled them to be dispersed well in a solution, which increased the stability and repeatability of fluorescence detection.

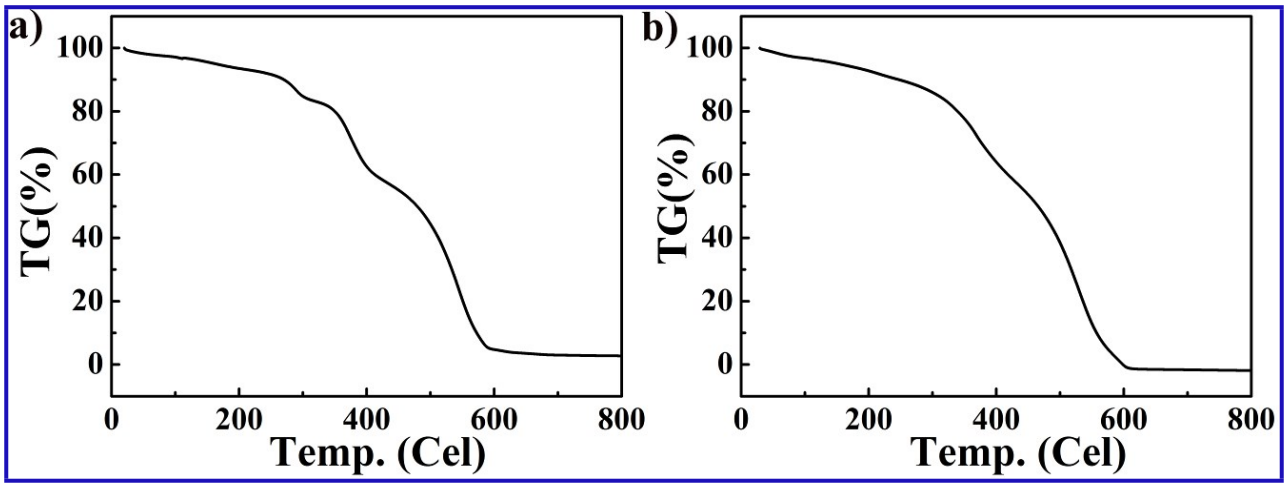

Fig. S13. a) Thermogravimetric analysis of COF_{BTT-Th} material, b) Thermogravimetric analysis of NCDs@COF_{BTT-Th} material.

According to the thermogravimetric analysis of COF_{BTT-Th} and NCDs@COF_{BTT-Th}, the thermal stability of the NCDs@COF_{BTT-Th} (the thermal decomposition temperature is 600 °C) was better than that of COF_{BTT-Th} (the thermal decomposition temperature is 580 °C) (Fig S12, Supporting Information). The good thermal stability might originate from the strong bonding between NCDs and $COF_{BTT-Th.}$ In addition, a slight weight loss at 200 °C occurred for COF_{BTT-Th}, but it did not occur for NCDs@COF_{BTT-Th}. It was probably due to the insertion of NCDs removed the solvent molecules in COF hole.

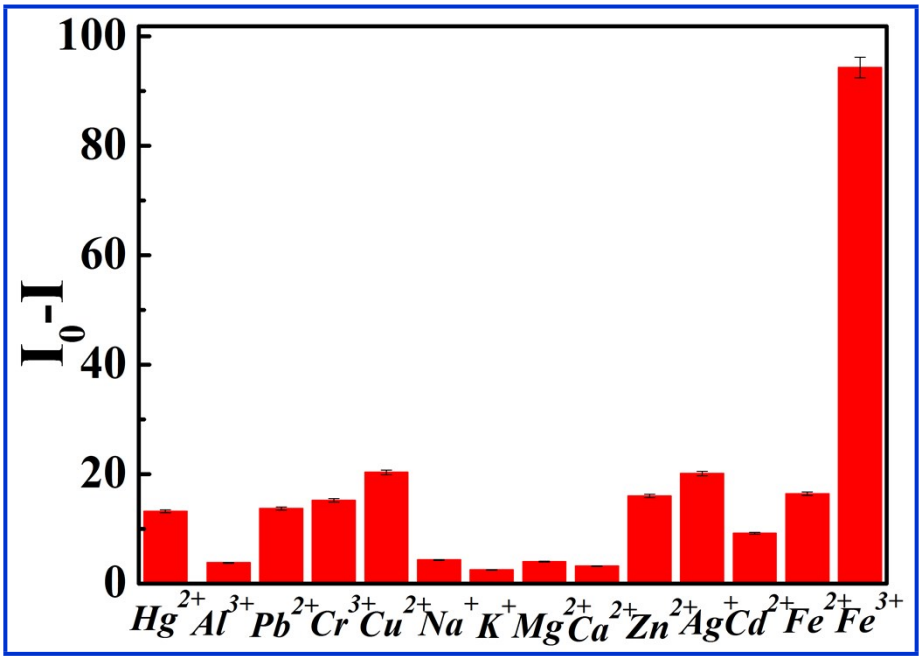

Fig. S14. Effect of various other metal ion (Hg^{2+}, Al^{3+}, Pb^{2+}, Cr^{3+}, Cu^{2+}, Na^{+}, K^{+}, Mg^{2+}, Ca^{2+}, Zn^{2+}, Ag^{+} , $Cd^{2+}$and Fe^{2+}) on the fluorescence intensity of NCDs@$COF_{BTT\text{-}Th}$. The concentration of all interfere cations is 100 μM except for Fe^{3+} (20 μM).

Selectivity is one of the important factors to be considered in the practical application of NCDs@$COF_{BTT\text{-}Th}$. Some common meta ions (including 100 μM Hg^{2+}, Al^{3+}, Pb^{2+}, Cr^{3+}, Cu^{2+}, Na^{+}, K^{+}, Mg^{2+}, Ca^{2+}, Zn^{2+}, Ag^{+}, $Cd^{2+}$and Fe^{2+}) was used to test the selectivity of NCDs@$COF_{BTT\text{-}Th}$. As shown in Fig S13, when the concentration of interference ions was 5 times of the Fe^{3+} concentration (20 μM), the interference effect was not very obvious. Such good selectivity provides possibilities for actual testing.

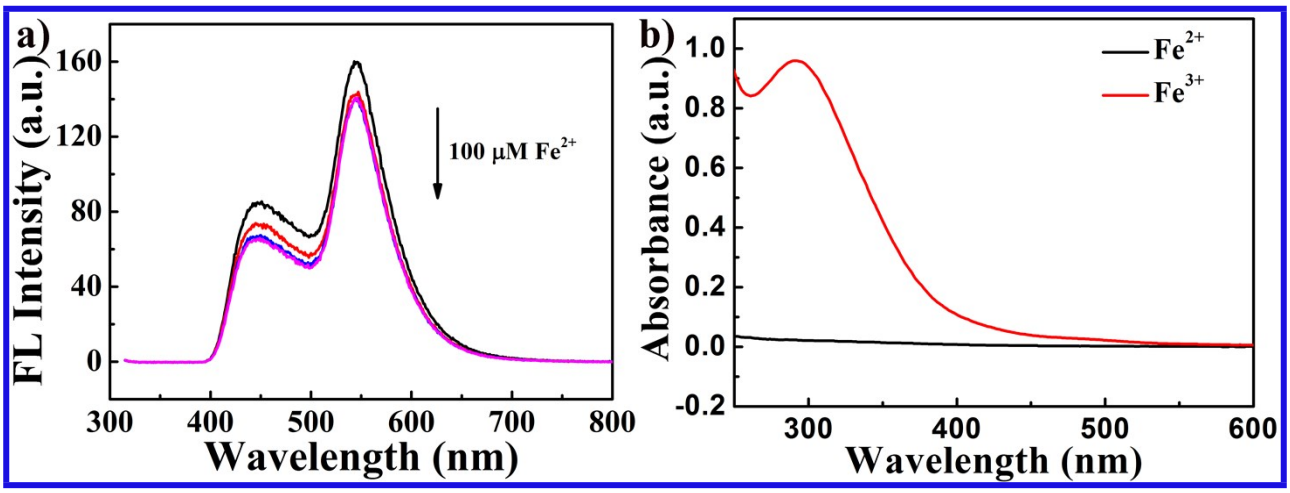

Fig. S15. a) Effect of Fe^{2+}on fluorescence intensity of NCDs@COF_{BTT-Th}; b) UV-vis absorption spectra of $Fe^{2+}$and Fe^{3+}.

The effect of Fe^{2+} on fluorescence intensity of NCDs@COF_{BTT-Th} is explored. As shown by Fig. S14a, Fe^{2+} does not basically affect on the fluorescence intensity of NCDs@COF_{BTT-Th}. It is probably related to the ultraviolet absorption of Fe^{2+}. It can be seen from the ultraviolet absorption of Fe^{2+} and Fe^{3+} that Fe^{2+} has no ultraviolet absorption at 300 nm (Fig. S14b), indicating that Fe^{2+} has little absorption of excitation wavelength.

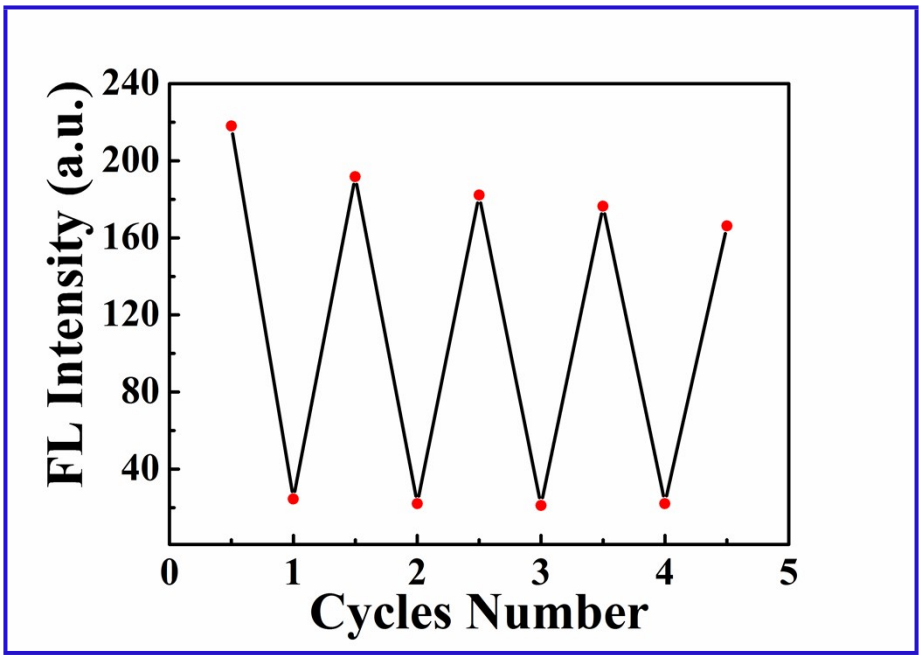

Fig. S16. Recycling use of NCDs@COF_{BTT-Th} for selective detection Fe^{3+}, Upon the treatment with EDTA solution, the NCDs@COF_{BTT-Th} can be repeatedly used.

We carried out recycling experiment of NCDs@COF_{BTT-Th} to test the reuse ability of NCDs@COF_{BTT-Th}. After the NCDs@COF_{BTT-Th} was used to test Fe^{3+}, EDTA solution was added to remove out the Fe^{3+}. NCDs@COF_{BTT-Th} was obtained by centrifugation at 10000 rpm again. The experimental result shows that the fluorescence of NCDs@COF_{BTT-Th} was enhanced after adding strong chelating agent EDTA solution to the suspension containing Fe^{3+} ions. After 4 cycles, the fluorescence of NCDs@COF_{BTT-Th} was not significantly lost, indicating that the material had a good recycling property.

Table S1. Recovery test of spiked Fe^{3+} in human serum samples with NCDs@COF_{BTT-Th}.

Samples	Atomic absorption/ μM	This method/ μM	Added / μM	Found/ μM	Recovery/ %
Serum 1	1.10	1.13	2	3.24	105.5
Serum 1	1.12	1.16	4	5.31	103.75
Serum 1	1.09	1.11	6	7.62	108.5

The human serum samples were diluted 10 times before experimental determination. Different volumes of Fe^{3+} standard solution were added to human serum samples. The solution was incubated for 30 min before fluorescence measurement, and the results detected by fluorescence sensor were consistent with that of atomic absorption spectrometry. Moreover, the recovery of Fe^{3+} in human serum samples reached 103.75%-108.5% (Table S1, Supporting Information). The above results indicated that the determination of Fe^{3+} by NCDs@COF_{BTT-Th} was of high accuracy and reliability.

References

1 Z. Gao, Z. Lin, X. Chen, H. Zhong, Z. Huang, *Anal. Methods,* 2016**,** ***8***, 2297-2304.

2 (a) H. Wei, J. Ning, X. Cao, X. Li, L. Hao, *J. Am. Chem. Soc.,* 2018, **140**, 11618-11622; (b) G. Das, D. Shinde, S. Kandambeth, B. Biswal, R. Banerjee, *Chem. Commun.,* 2014, **50**, 12615-12618.

3 (a) L. Wang, G. Fang, D. Cao, *Sens. Actuators, B,* 2015, **207**, 849-857; (b) M. Gao, P. Xie, L. Wang, X. Miao, F. Guo, *Res. Chem. Intermed.,* 2015, **41**, 9673-9685.

4 (a) Y. Wu, G. Yang, X. Zhou, J. Li, Y. Ning, Y. Wang, *Dalton Trans.,* 2015, **44**, 10385-10391; (b) Y. Dai, J. Fu, K. Yao, Q. Song, K. Xu, X. Pang, *Spectrochim, Acta, Part A,* 2018, **192**, 257-262.

5 (a) R. Atchudan, T. Edison, K. Aseer, S. Perumal, N. Karthik, Y. Lee, *Biosens. Bioelectron.,* 2018, **99**, 303-311; (b) K. Kaur, S. Chaudhary, S. Singh, S. Mehta, *Sens. Actuators, B,* 2016, **232**, 396-401; (c) L. Fan, Y. Wang, L. Li, J.Zhou, *Colloids Surf. A,* 2020, **588**, 124378.

6 (a) L. Chen, C. Wu, P. Du, X. Feng, P. Wu, C. Cai, *Talanta,* 2017, **164**, 100-109; (b) J. Wang, M. Jiang, L. Yan, R. Peng, M. Huang, X. Guo, Y. Li, P. Wu, *Inorg. Chem.,* 2016, **55**, 12660-12668; (c) N. Sharma, S. Reja, N. Gupta, V. Bhalla, D. Kaur, S. Arora, M. Kumar, *Org. Biomol. Chem.,* 2017, **15**, 1006-1012.